Crop and Environment 2 (2023) 24–36

Contents lists available at ScienceDirect

Crop and Environment

journal homepage: www.journals.elsevier.com/crop-and-environment

Original Article

Enhancing leaf photosynthesis from altered chlorophyll content requires optimal partitioning of nitrogen

Zhenxiang Zhou [a], Paul C. Struik [a], Junfei Gu [b], Peter E.L. van der Putten [a], Zhiqin Wang [b], Xinyou Yin [a,**], Jianchang Yang [b,*]

[a] Centre for Crop Systems Analysis, Department of Plant Sciences, Wageningen University & Research, PO Box 430, 6700 AK Wageningen, the Netherlands
[b] College of Agriculture, Yangzhou University, 48 Wenhui East Road, Yangzhou, Jiangsu, 225009, China

ARTICLE INFO

Keywords:
Chlorophyll content
Light energy utilisation efficiency
Nitrogen partitioning
Non-photochemical quenching
Oryza sativa
Photosynthetic capacity

ABSTRACT

While optimising leaf chlorophyll content ([CHL]) has been proposed as a relevant means to manipulate canopy light penetration and canopy photosynthesis, effects of modifying [CHL] on leaf photosynthesis are yet to be investigated thoroughly. A greenhouse experiment and a field experiment were conducted involving rice genotypes of different genetic backgrounds and their leaf-colour variants. Leaf photosynthesis was more influenced by alteration to yellow-leaf than to stay-green cases. Higher specific leaf area and stomatal conductance were observed in two yellow-leaf variants, while only one yellow-leaf variant showed significantly increased Rubisco carboxylation capacity (V_{cmax}), maximum electron transport rate (J_{max}), and photosynthetic nitrogen-use efficiency (PNUE). Model analysis indicated that reducing leaf [CHL] decreased the energy loss via non-photochemical quenching, but improving V_{cmax}, J_{max}, and PNUE would require an improved nitrogen distribution pattern within the leaf. Label-free quantitative proteomics confirmed that an increased investment of nitrogen in Cyt b_6/f and Rubisco was observed in the yellow-leaf variant of the genetic background with improved V_{cmax}, J_{max}, and PNUE, but not in the other background. Our results suggest that reducing [CHL] can improve leaf photosynthesis only if the saved nitrogen is optimally distributed to proteins that are more rate-limiting to photosynthesis.

1. Introduction

Research on exploring ways to improve photosynthesis has never been to a standstill. Since the 1960s, stay-green, known as increased duration of greenness, has been well-established as a superior trait in extending photosynthesis (especially during grain filling) and thus improves crop yield (Borrell et al., 2014; Gregersen et al., 2013; Thomas and Ougham, 2014). Soon afterwards, a deceptively linear relationship between nitrogen (N) content, leaf greenness, and crop yield from empirical cultivation made farmers continuously increase the input of N resources, which forced the leaf greenness into a saturated level (Swain and Sandip, 2010; Wood et al., 1993). In fact, for a long time breeders also tended to select greener leaves with the hope to improve photosynthesis (Hossain and Fischer, 1995; Khush, 1995).

Leaf greenness is determined by the concentration of chlorophyll molecules ([CHL]). Genotypes with greener leaves would mean that most of the incoming irradiance (ca. 70%) is intercepted by upper leaves in a canopy (Song et al., 2013), while lower leaves are being shaded and probably contribute less to canopy productivity. Therefore, more recently, optimising [CHL] to increase light penetration to lower layers in a canopy was proposed to improve canopy photosynthesis (Ort et al., 2011). A number of studies (Song et al., 2017; Walker et al., 2018) have explored the potential of using light-green or yellow variant genotypes in improving canopy photosynthesis. However, canopy photosynthesis is the sum of photosynthetic rates of individual leaves in the stand. While exploring the potential to improve canopy photosynthesis, one cannot bypass the impact of modifying [CHL] on leaf photosynthesis per se.

Theoretically, when other components are kept constant, the impact of modifying [CHL] on leaf photosynthesis can be reflected at least in two ways: (i) altered non-photochemical quenching (NPQ) due to changes in absorbed energy and (ii) altered leaf N distribution pattern. The NPQ, which serves not only as one of the leaf photo-protective mechanisms but also as one of the energy decay paths, competes with photochemical processes for the light energy absorbed by leaves (Ruban, 2016). This

* Corresponding author.
** Corresponding author.
E-mail addresses: xinyou.yin@wur.nl (X. Yin), jcyang@yzu.edu.cn (J. Yang).

https://doi.org/10.1016/j.crope.2023.02.001
Received 6 December 2022; Received in revised form 1 February 2023; Accepted 8 February 2023

decay path is often present when the absorbed light intensity of (greener) leaves is higher than the capacity of energy utilisation by the photosynthetic metabolisms. For C_3 plants, solar conversion efficiency is negatively correlated with irradiance and photosynthesis may become saturated at a quarter of maximum full sunlight (Melis, 2009). Excessive light will give rise to undue excitation beyond the maximal capacity for photochemical reactions in leaves, which may result in damage to Photosystem II (PSII) (Krieger-Liszkay et al., 2008; Takagi et al., 2016). Under these circumstances, it would be unwise to continue breeding green-leaf crops for higher photosynthetic potential. Instead, making leaf colour lighter may result in lower requirement to engage NPQ for dissipating excessive energy (Kirst et al., 2017; Melis, 2009) and higher 'work efficiency' of individual chlorophyll molecules (Gilmore and Ball, 2000; Kirst et al., 2018). However, whether lighter-coloured leaves would always be associated with the alteration of NPQ and whether the capacity of photochemical energy utilisation could be improved if less light energy is dissipated via NPQ in light-green leaves remain to be quantified.

More importantly, modifying leaf greenness provides the chance to save N from excessive [CHL] to be invested in other more rate-limiting photosynthetic proteins. Many studies have shown that partitioning of leaf photosynthetic N (N_{photo}) among the elements of the photosynthetic apparatus is suboptimal, and the N investment in chlorophyll molecules is superfluous and can be saved for other purposes (Polle et al., 2002; Slattery et al., 2017; Walker et al., 2018). In a typical plant photosystem, only ca. 25% of the chlorophyll molecules are needed to maintain the stable operation of photosynthetic electron transport (Glick and Melis, 1988). Under high-light conditions, the energy harvested by the chlorophyll-protein complex is far more than the capacity of energy that can be utilised by the photosynthetic metabolisms. So, a lower leaf [CHL] in top leaves to lower light absorptance and NPQ may serve the purpose of optimising leaf N allocation. It is expected that a decreased leaf [CHL] might improve parameters such as the maximum carboxylation capacity of Rubisco (V_{cmax}) and the maximum electron transport rate under saturated light (J_{max}), which often limit the top-leaf photosynthetic capacity. As a result, leaf photosynthetic N-use efficiency (PNUE) can also be expected to increase. However, so far, there is no evidence that saved N from reduced [CHL] will result in an improved photosynthetic N allocation.

Given that the concept of a reduced leaf [CHL] fundamentally differs from the traditional recommendation by crop physiologists for stay-green traits (i.e. sustaining the green colour and photosynthetic competence during later grain filling stage), comparing the effects of these contrasting leaf-colour traits could therefore help better explore the opportunities of further improving photosynthesis by modifying leaf [CHL]. In this study, we used four rice cultivars, in which each cultivar had modified [CHL] to have leaves that were either yellower or greener than the default type. We intended to examine (i) the relationship between NPQ and modified [CHL]; (ii) whether modifying leaf [CHL] might improve the N partitioning and thus leaf photosynthesis; and (iii) if so, whether these effects depend on cultivar backgrounds.

2. Materials and methods

2.1. Plant materials

Our rice (*Oryza sativa* L.) materials were derived from four background groups and each group was modified for either greener or yellower or both leaf colours, resulting in a total of nine genotypes (Table 1). Two groups (cv. Guanglingxiangnuo, abbreviated as "GLXN"; and cv. Yandao 8, abbreviated as "YD") belonged to mid-season *japonica* rice material, of which GLXN was modified via tissue culture (a T-DNA insertion variant carrying the *Wx* gene relating to amylose content, see Liu et al. 2014) and YD was modified via radiation mutagenesis (with ^{60}Co γ-rays), to have stay-green leaves. The other two groups of rice materials were also obtained by radiation mutagenesis (with ^{60}Co γ-rays): one group of rice material (cv. Wuyunjing 3, abbreviated as "WYJ") belonged to a *japonica* type and was modified to have either greener or yellower leaves; the other group was early *indica* rice material (cv. Zhefu 802, abbreviated as "ZF") and was modified to have the yellower leaves. Resulting stay-green and yellower genotypes were marked as G and Y, respectively, while the nonmodified or default genotypes were labelled as CK (Table 1). Seeds of GLXN, YD, WYJ, and their variant genotypes were from Yangzhou University and seeds of ZF and its variant genotype were from Zhejiang University, China. Our pre-experiments, in which these genotypes were grown for several generations, have shown the stability of the G and Y variant lines.

Table 1
Rice genotypes of four genetic backgrounds used in this study as a result of modifying leaf chlorophyll content of the default genotype (CK) into either greener-leaf (G) or yellower-leaf (Y) variants.

Background	Genotype	Abbreviation	Characteristics
Guanglingxiangnuo	Default control	GLXN-CK	a mid-season *japonica* rice cultivar with high grain quality
	Stay-green variant	GLXN-G	a form of GLXN from tissue culture with stay-green trait
Yandao 8	Default control	YD-CK	a mid-season *japonica* rice cultivar
	Stay-green variant	YD-G	a radiation mutagenesis form of YD with stay-green trait
Wuyunjing 3	Default control	WYJ-CK	a *japonica* rice cultivar
	Stay-green variant	WYJ-G	a radiation mutagenesis form of WYJ with stay-green trait
	Yellow-leaf variant	WYJ-Y	a radiation mutagenesis form of WYJ with yellow leaves
Zhefu 802	Default control	ZF-CK	an early *indica* rice cultivar
	Yellow-leaf variant	ZF-Y	a radiation mutagenesis form of ZF with light-green leaves

2.2. Greenhouse experiment and measurements

A greenhouse experiment was conducted at Wageningen University & Research, Wageningen, the Netherlands (51°58′N, 05°40′E). Temperature was set at 26°C (12 h during daytime) and 23°C (12 h during night time). The CO_2 level was about 400 μmol mol^{-1} and the relative humidity was set at 65%. Extra SON-T lights were switched on when incoming solar radiation intensity outside the greenhouse became less than 400 W m^{-2} and then switched off once it exceeded 500 W m^{-2}. Pre-germinated seeds of the nine genotypes were sown in porous plastic trays (filled with nutrition-rich substrate) twice, on April 10 and 17, 2019, to spread out time windows for measurement. Seedlings were then transplanted to pots (24 cm in diameter, 20 cm in height, and 7 L in volume) at the three-leaf stage with two seedlings per pot. Each pot contained 6.5 kg of sandy loam soil with 84.5 mg alkali-hydrolysable N, 6.5 mg Olsen-P, and 229.7 mg exchangeable K. All pots were placed on movable lorries according to a randomised complete block design with three replications per genotype. One day before transplanting, 1.5 g KH_2PO_4 and 0.5 g urea per pot as basal fertiliser were pre-mixed through the soil. Extra N fertilisers were split-applied at early tillering stage (0.2 g urea per pot) and at panicle initiation stage (0.3 g urea per pot).

Photosynthesis measurements were conducted at stem-elongating (2nd leaf from the top), flowering (flag leaf), and grain-filling (ca. 20 d after flowering, flag leaf) stages. Pre-labelled and fully expanded leaves on the main stems of four representative plants of each genotype were chosen for measurements. An open-path gas exchange system integrated with a fluorescence chamber head (Li-Cor 6800, Li-Cor Inc., Lincoln, NE, USA) was used to simultaneously measure gas exchange and chlorophyll fluorescence parameters. All measurements were carried out at a leaf

temperature of 25°C and a leaf-to-air vapour pressure deficit between 1.0 and 1.6 kPa.

Light and CO_2 response curves were measured at the same position of the leaves. Prior to measurements of light response curves, leaves were acclimated to initial incident irradiance (I_{inc}) setting of 2,000 μmol m^{-2} s^{-1} (for ca. 30 min) until the net CO_2 assimilation rate (A) was stable. Then the automatic programming was operated with I_{inc} in the leaf cuvette in a decreasing series: 2,000, 1,500, 1,000, 500, 280, 150, 100, 80, and 50 μmol m^{-2} s^{-1} (6–8 min per step), while keeping ambient CO_2 level (C_a) at 400 μmol mol^{-1}. The CO_2 response curves were measured at I_{inc} of 1,000 μmol m^{-2} s^{-1}, with the C_a steps: 400, 250, 150, 80, 50, 400, 400, 400, 650, 1,000, and 1,500 μmol mol^{-1} (3–5 min per step, but note that using the three repeated 400 μmol mol^{-1} was merely to re-adapt leaves and the data from these three points were excluded in analysis). The above two curves were measured at ambient O_2 (21%) level. To convert fluorescence-based Photosystem II (PSII) photochemical efficiency into electron transport flux, we also conducted the measurements under non-photorespiratory conditions (2% O_2 combined with C_a at 1,000 μmol mol^{-1}) to establish a calibration curve. The low O_2 level was realised by using a cylinder containing a gas mixture of 2% O_2 and 98% N_2. Under this circumstance, only half of the light response curve was measured with I_{inc} being 280, 150, 100, 80, and 50 μmol m^{-2} s^{-1}, to ensure that data used for calibration were within the electron transport-limited range. All gas exchange data were corrected for basal leakage of CO_2 into and out of the leaf cuvette, based on measurements on boiled leaves across the same range of CO_2 levels, and intercellular CO_2 levels (C_i) were then re-calculated. The flow rate for all measurements was 400 μmol s^{-1}.

The dark-adapted maximum fluorescence yields (F_m) were measured after the plants had been placed in the darkness for the whole night. For measurements at each irradiance or CO_2 step of the response curves, the steady-state fluorescence (Fs) was recorded after A reached the steady state. At the same time, the maximum fluorescence under light-adapted condition (F'_m) was determined using a multiphase flash method (Loriaux et al., 2013): each of the three phases went through a duration of 300 ms and flash intensity of 6,500 μmol m^{-2} s^{-1} in the second phase was attenuated by 40%. The apparent operating photochemical efficiency of PSII was derived as $\Phi_2 = 1 - F_s/F'_m$ (Genty et al., 1989). The NPQ was calculated as NPQ $= F_m/F'_m - 1$ (Bilger and Björkman, 1990; Ruban, 2016).

All leaf segments used for photosynthesis measurements were cut out and used immediately to measure the leaf area with a LI-3100 area meter (Li-Cor, Lincoln, NE, USA), the values for SPAD using a chlorophyll meter (SPAD-502, Minolta Camera Co., Japan), and light absorptance (β) using a spectrometer (STS-VIS miniature spectrometer, Ocean Optics, USA). All leaf materials were then oven-dried at 70°C for 48 h to constant weight. Specific leaf area (SLA) was calculated as the leaf area to leaf mass ratio. Each leaf segment was ground into powder in a 2 ml centrifuge tube, which was used to measure the N content by an element analyser based on the micro-Dumas combustion method. Specific leaf N (SLN, in g N m^{-2}) was then calculated.

2.3. Field experiment and measurements

A field experiment was conducted at Yangzhou University, Jiangsu Province, China (32°30′N, 119°25′E) during the rice growing season from May to November 2020. The soil used in the experiment was a sandy loam (Typic Fluvaquent, Etisols (U.S. taxonomy)) with 25.5 g kg^{-1} organic matter, 103 mg kg^{-1} alkali-hydrolysable N, 33.4 mg kg^{-1} Olsen-P, and 70.5 mg kg^{-1} exchangeable K. The seeds were first sown in the paddy seedbed field plots on May 27, 2020. The seedlings were then transplanted to the experimental field on June 23, 2020 with a hill spacing of 0.25 m × 0.16 m and two seedlings $hill^{-1}$. A split-plot design was used with main plots for the genetic backgrounds and subplots for genotypes in a randomised block arrangement with three replicates. The main plots were separated by ridges at a 1 m width covered by plastic film inserted in the soil at a depth of 0.5 m. Every split-plot area was 20 m^2, and the size of each main plot for the WYJ background (having three genotypes, Table 1) was 60 m^2 while it was 40 m^2 for each of the other three backgrounds (i.e. GLXN, YD, and ZF). For fertiliser management, N

Table 2
List of model symbols and the definition and unit of each symbol.

Symbol	Definition	Unit
A	Net photosynthesis rate	μmol CO_2 m^{-2} s^{-1}
A_c	Rubisco activity limited net photosynthesis rate	μmol CO_2 m^{-2} s^{-1}
A_j	Electron transport limited net photosynthesis rate	μmol CO_2 m^{-2} s^{-1}
A_p	Triose phosphate utilisation limited net photosynthesis rate	μmol CO_2 m^{-2} s^{-1}
A_{max}	Maximum net photosynthesis rate under saturated light situation at ambient CO_2 level	μmol CO_2 m^{-2} s^{-1}
C_a	Ambient air CO_2 concentration	μmol mol^{-1}
C_c	Chloroplast CO_2 partial pressure	μbar
C_i	Intercellular CO_2 partial pressure	μbar
CE	Carboxylation efficiency of Rubisco, described by the initial slope of the A-C_i curve	mol m^{-2} s^{-1} bar^{-1}
F_{npq}	Fraction of the energy flow that is lost via NPQ	–
g_s	Stomatal conductance for CO_2	mol m^{-2} s^{-1}
g_m	Mesophyll diffusion conductance	mol m^{-2} s^{-1} bar^{-1}
g_{mo}	Residual mesophyll diffusion conductance in the g_m model	mol m^{-2} s^{-1} bar^{-1}
I_{inc}	Photon flux density incident to leaves	μmol photons m^{-2} s^{-1}
I_{abs}	Photon flux density absorbed by leaf photosynthetic pigments	μmol photons m^{-2} s^{-1}
I_{50}	Photon flux density incident to leaves when $J_{NPQ} = J_2$	μmol photons m^{-2} s^{-1}
J	Linear electron transport rate through PSII	μmol e^- m^{-2} s^{-1}
J_2	Rate of all (i.e. linear plus pseudocyclic) electron transport through PSII	μmol e^- m^{-2} s^{-1}
J_{NPQ}	Rate of an electron-equivalent flux through PSII used for NPQ	μmol e^- m^{-2} s^{-1}
J_{50}	Value of J when $J_{NPQ} = J_2$	μmol e^- m^{-2} s^{-1}
J_{max}	Maximum value of J under saturated light	μmol e^- m^{-2} s^{-1}
K_{mC}	Michaelis–Menten constant of Rubisco for CO_2	μbar
K_{mO}	Michaelis–Menten constant of Rubisco for O_2	mbar
O	Oxygen partial pressure	mbar
R_d	Day respiration (i.e. respiratory CO_2 release other than by photorespiration)	μmol CO_2 m^{-2} s^{-1}
s	Slope factor for linear regression of A versus $I_{inc}\Phi_2/4$ under nonphotorespiratory conditions	–
s'	Slope factor for linear regression of A versus $I_{inc}\Phi_2/4$ under photorespiratory conditions	–
$S_{c/o}$	Relative CO_2/O_2 specificity factor for Rubisco	mbar μbar^{-1}
T_p	Rate of triose phosphate (TP) utilisation	μmol TP m^{-2} s^{-1}
V_{cmax}	Maximum rate of carboxylation by Rubisco	μmol CO_2 m^{-2} s^{-1}
α_2	Quantum efficiency of PSII e^- transport on the leaf pigment-absorbed light (i.e. I_{abs}) basis	mol e^- (mol photons)$^{-1}$
α_{2LL}	Value of α_2 at strictly limiting light	mol e^- (mol photons)$^{-1}$
β	Absorptance by leaf photosynthetic pigments	–
$\Gamma*$	C_c-based CO_2 compensation point in the absence of R_d ($= 0.5O/S_{c/o}$)	μbar
δ	A parameter in the g_m model	–
θ	Convexity factor for response of J to I_{inc}	–
κ_2	Conversion efficiency of incident light (i.e. I_{inc}) into J	mol e^- (mol photons)$^{-1}$
κ_{2LL}	Value of κ_2 at strictly limiting light	mol e^- (mol photons)$^{-1}$
ρ_2	Proportion of I_{abs} partitioned to PSII	–
Φ_2	Quantum efficiency of PSII e^- flow on PSII-absorbed light basis	mol e^- (mol photons)$^{-1}$
Φ_{2LL}	Value of Φ_2 at the strictly limiting light level	mol e^- (mol photons)$^{-1}$
$\Phi_{CO2LL(inc)}$	Quantum yield of CO_2 assimilation on the basis of I_{inc}	mol CO_2 (mol photons)$^{-1}$
$\Phi_{CO2LL(abs)}$	Quantum yield of CO_2 assimilation on the basis of I_{abs}	mol CO_2 (mol photons)$^{-1}$

(120 kg N ha^{-1} as urea), phosphorus (30 kg ha^{-1} as single superphosphate), and potassium (40 kg ha^{-1} as KCl) as basal fertiliser were applied just before transplanting. A total of additional 120 kg N ha^{-1}, again in the form of urea, was applied at the stages of early tillering and panicle initiation (4:6). The proportions of urea application across stages were the same as in the greenhouse study.

The SPAD values and SLN data were measured as described for the greenhouse experiment. The leaf [CHL] was measured only in the field experiment according to the method of Arnon (1949). The newly expanded leaves were ground to extract chlorophyll with 95% ethanol at 60–65°C and then the chlorophyll content was determined using an ultraviolet spectrophotometer (Lambda 650, PerkinElmer, USA). Maximum net photosynthesis rate at the ambient CO_2 level (A_{max}) was measured under saturated light (2,000 μmol m^{-2} s^{-1}) using an open-path gas exchange system (Li-Cor 6400XT, Li-Cor Inc., Lincoln, NE, USA) at flowering stage. Other environmental conditions were set as for the measurements in the greenhouse experiment.

Part of leaf materials sampled after photosynthesis measurements were stored in liquid N for proteomic measurements. A quantitative proteomic analysis was conducted following the same procedure as described by Cui et al. (2021) and Zhou et al. (2021). This included the steps of sample preparation, protein extraction, protein extraction quality control, protein enzymatic hydrolysis, high pH reversed-phase peptide separation, data dependent acquisition (DDA), data independent acquisition (DIA) analysis by nano-LC-MS/MS, and bioinformatics analysis. All sample data were generated from a high-resolution mass spectrometer (Thermo Fisher Scientific, CA, USA) and protein identification was performed using a database consisting of the rice proteome, which was downloaded from UniProt (https://www.uniprot.org/). DDA data were identified by the Andromeda search engine within MaxQuant (V. 1.5.3.30) (Cox and Mann, 2008) and identification results were used for spectral library construction with the false discovery rate (FDR) being set at 1% for protein and peptides. For large-scale DIA data, the mProphet algorithm in Spectronaut (12.0.20491.14.21367) software was used to complete analytical quality control, thus obtaining a large number of reliable quantitative results. Statistical evaluation of significant differences in proteins or peptides was carried out using the "MSstats" package in R with its core algorithm being a linear mixed effect model. Then the significance test was performed according to the predefined comparison group. Differential protein screening was performed based on the Log_2 (Foldchange) > 1 and $P < 0.05$ as the criterion for the significant difference. At the same time, an enrichment analysis was performed on the differential proteins.

2.4. Estimating photosynthesis parameters

We used the model from Farquhar et al. (1980) ('FvCB model', see Supplementary Appendix A) to analyse the data for net photosynthetic rate (A, see Table 2 for the explanation of all model symbols). Model parameters were estimated according to the step-wise procedures described by Yin et al. (2009). First, the apparent quantum efficiency of PSII electron transport under strictly limiting light (Φ_{2LL}) was estimated by extrapolating data for the light response of Φ_2 to the zero light, using the method of Yin et al. (2009). Next, a linear regression plot of electron transport-limited photosynthetic rate, A_j, against ($I_{inc}\Phi_2/4$) was made using data from limiting light under non-photorespiratory condition (NPR):

$$A_j = s(I_{inc}\Phi_2 / 4) - R_d \quad (1)$$

where the intercept of this linear regression provides an estimate of day respiration (R_d) (also see Yin et al., 2011) while the slope s can be used to calculate the conversion efficiency of I_{inc} into electron transport under limiting-light conditions, κ_{2LL} (see Eqn A3b from Supplementary Appendix A):

Table 3
Values (standard errors of mean in brackets if applicable) of photosynthetic parameters for four default rice genotypes (CK) and their greener-leaf variants (G) or yellower-leaf variants (Y) at three stages. Genotypes codes are explained in Table 1. Parameter definitions and units are given in Table 2 or in the text. δ was estimated from the data of the A_j-limited part of both A-I_{inc} and A-C_i curves, i.e. low I_{inc} range of light response curves: 150, 100, 80, and 50 μmol m^{-2} s^{-1} for both 21% O_2 and 2% O_2 and high C_a range of CO_2 response curve: 650, 1,000, and 1,500 μmol mol^{-1}. J_{max}, V_{cmax}, and T_p were estimated from gas exchange data only based on pre-calculated δ by the g_m model.

Stage	Background	Genotype	FvCB model parameters						Other parameters	
			R_d	κ_{2LL}	δ^a	J_{max}	V_{cmax}	T_p	Φ_{2LL}	s
Stem-elongating	GLXN	CK	0.758	0.296	0.944 (0.060)	155.3 (3.6)	131.9 (5.3)	7.2 (0.08)	0.731 (0.006)	0.405 (0.006)
		G	0.612	0.258		135.1 (4.1)	101.8 (2.8)	6.5 (0.14)	0.728 (0.008)	0.354 (0.006)
	YD	CK	0.673	0.280		171.1 (4.2)	139.5 (2.7)	8.7 (0.14)	0.696 (0.012)	0.403 (0.005)
		G	0.706	0.297		195.4 (4.6)	145.6 (2.1)	9.0 (0.14)	0.717 (0.007)	0.414 (0.010)
	WYJ	CK	0.982	0.274		201.1 (5.1)	153.6 (2.9)	9.2 (0.14)	0.615 (0.035)	0.446 (0.015)
		G	0.790	0.275		202.1 (5.2)	150.0 (2.7)	8.5 (0.12)	0.704 (0.013)	0.391 (0.013)
		Y	0.824	0.154		203.3 (9.1)	153.8 (27.9)	7.5 (0.11)	0.594 (0.013)	0.259 (0.007)
	ZF	CK	0.629	0.266		120.8 (4.2)	90.1 (2.1)	6.7 (0.18)	0.710 (0.005)	0.375 (0.006)
		Y	0.740	0.235		169.4 (4.2)	137.2 (4.1)	7.7 (0.11)	0.691 (0.007)	0.341 (0.005)
Flowering	GLXN	CK	0.643	0.276	0.788 (0.056)	137.8 (5.0)	130.9 (4.2)	6.4 (0.09)	0.730 (0.005)	0.378 (0.009)
		G	0.468	0.246		126.4 (5.2)	114.0 (4.1)	5.7 (0.09)	0.711 (0.008)	0.346 (0.007)
	YD	CK	0.769	0.310		228.4 (6.5)	193.8 (6.2)	9.7 (0.10)	0.673 (0.013)	0.461 (0.011)
		G	0.902	0.304		238.4 (6.8)	203.2 (6.3)	9.9 (0.09)	0.688 (0.003)	0.443 (0.009)
	WYJ	CK	0.674	0.307		241.4 (6.9)	201.4 (5.2)	9.9 (0.09)	0.713 (0.006)	0.431 (0.004)
		G	0.883	0.298		254.5 (7.8)	198.2 (6.3)	9.9 (0.10)	0.708 (0.004)	0.421 (0.004)
		Y	0.757	0.182		232.8 (10.8)	200.9 (29.8)	9.0 (0.10)	0.619 (0.009)	0.294 (0.007)
	ZF	CK	0.753	0.284		157.7 (5.4)	126.9 (2.8)	8.2 (0.16)	0.714 (0.007)	0.398 (0.005)
		Y	1.025	0.251		282.5 (9.8)	217.8 (11.9)	10.9 (0.10)	0.698 (0.004)	0.360 (0.004)
20 d after flowering	GLXN	CK	0.557	0.246	1.200 (0.072)	70.0 (2.0)	48.6 (1.4)	4.5 (0.14)	0.725 (0.013)	0.339 (0.006)
		G	0.380	0.231		64.2 (2.1)	40.2 (1.3)	4.3 (0.20)	0.733 (0.020)	0.315 (0.006)
	YD	CK	0.612	0.257		81.7 (2.1)	51.8 (1.4)	5.4 (0.23)	0.683 (0.027)	0.377 (0.012)
		G	0.531	0.282		96.0 (1.7)	65.5 (4.0)	5.4 (0.14)	0.675 (0.035)	0.418 (0.004)
	WYJ	CK	0.464	0.252		80.7 (1.6)	62.9 (3.0)	4.8 (0.14)	0.703 (0.009)	0.359 (0.010)
		G	0.382	0.246		81.0 (2.0)	54.9 (1.5)	5.1 (0.20)	0.720 (0.011)	0.341 (0.010)
		Y	0.497	0.131		104.2 (2.8)	72.7 (2.5)	5.3 (0.16)	0.627 (0.020)	0.210 (0.013)
	ZF	CK	0.486	0.204		58.7 (2.0)	37.1 (1.3)	4.2 (0.13)	0.650 (0.027)	0.314 (0.008)
		Y	0.576	0.188		95.4 (2.2)	67.7 (4.5)	5.4 (0.16)	0.680 (0.009)	0.277 (0.007)

[a] The estimate δ did not vary significantly among genotypes within each stage, so a common value was estimated for a given stage (see the text).

$$\kappa_{2LL} = s\Phi_{2LL} \quad (2)$$

The slope factor s of Eqn (1) is also as a calibration factor, with which fluorescence-based Φ_2 can be converted into the potential linear electron transport rate used for CO_2 fixation and photorespiration (J) under all conditions (Yin et al. 2009):

$$J = sI_{inc}\Phi_2 \quad (3)$$

The calculated J values along the light response curves were fitted to Eqn (A3b) of Supplementary Appendix A to estimate fluorescence-based J_{max} (the maximum value of J under saturated light) and the curve factor θ. When fitting Eqn (A3b), we found that the curvature factor θ did not vary much, and we therefore estimated a common θ (0.76) for all nine genotypes and three measurement stages. This also allowed a better comparison of parameter J_{max} among the genotypes and stages.

In order to examine whether mesophyll conductance for CO_2 diffusion (g_m) varied with I_{inc} and C_i level, a variable J method from Harley et al. (1992) was first applied to calculate g_m. This analysis showed that g_m is variable and declines with increasing C_i and decreasing I_{inc} (results not shown). Therefore, we used an equation of Yin et al. (2009) to model variable g_m: $g_m = g_{mo} + \delta(A + R_d)/(C_c - \Gamma_*)$, where g_{mo} represents the minimum mesophyll conductance as I_{inc} is close to zero (set to zero here according to the result of the variable J method). Parameter δ is the dimensionless coefficient that can accommodate a variable-g_m mode and its value actually represents the carboxylation resistance to mesophyll resistance ratio (Yin et al., 2020). C_c is the chloroplast partial pressure of CO_2 and Γ^* is the C_c-based CO_2 compensation point in the absence of R_d. Then, this equation was combined with Eqns (A2) and (A3a) and C_c was replaced by (C_i–A/g_m) to solve for A_c (Rubisco-limited rate of net photosynthetic rate) and A_j (Yin et al., 2009):

$$A_c \text{ or } A_j = \left(-b - \sqrt{b^2 - 4ac}\right) \Big/ (2a) \quad (4)$$

where $a = x_2 + \Gamma_* + \delta(C_i + x_2)$

$$b = -\{(x_2 + \Gamma_*)(x_1 - R_d) + (C_i + x_2)[g_{mo}(x_2 + \Gamma_*) + \delta(x_1 - R_d)] + \delta[x_1(C_i - \Gamma_*) - R_d(C_i + x_2)]\}$$

$$c = [g_{mo}(x_2 + \Gamma_*) + \delta(x_1 - R_d)][x_1(C_i - \Gamma_*) - R_d(C_i + x_2)]$$

$$\text{with } x_1 = \begin{cases} V_{cmax} & \text{for } A_c \\ J/4 & \text{for } A_j \end{cases}$$

$$x_2 = \begin{cases} K_{mC}(1 + O/K_{mO}) & \text{for } A_c \\ 2\Gamma_* & \text{for } A_j \end{cases}$$

To avoid overfitting, δ was calculated beforehand using data from the A_j-limited range (i.e. both low I_{inc} range of light response curves and high C_i range of CO_2-response curves) by combining Eqn (4) with Eqn (3). Then, J_{max}, V_{cmax}, and T_p (the rate of triose phosphate utilisation) can be estimated simultaneously by fitting combined Eqn (A1), Eqn (A3b), Eqn (A4), and Eqn (4) to all CO_2 exchange data. For all these analyses, we used the values of Rubisco parameters measured at 25°C by Cousins et al. (2010): 3.022 mbar μbar^{-1} for $S_{c/o}$ (the relative CO_2/O_2 specificity factor for Rubisco), 291 μbar for K_{mC} (Michaelis-Menten constant of Rubisco for CO_2), and 194 mbar for K_{mO} (Michaelis-Menten constant of Rubisco for

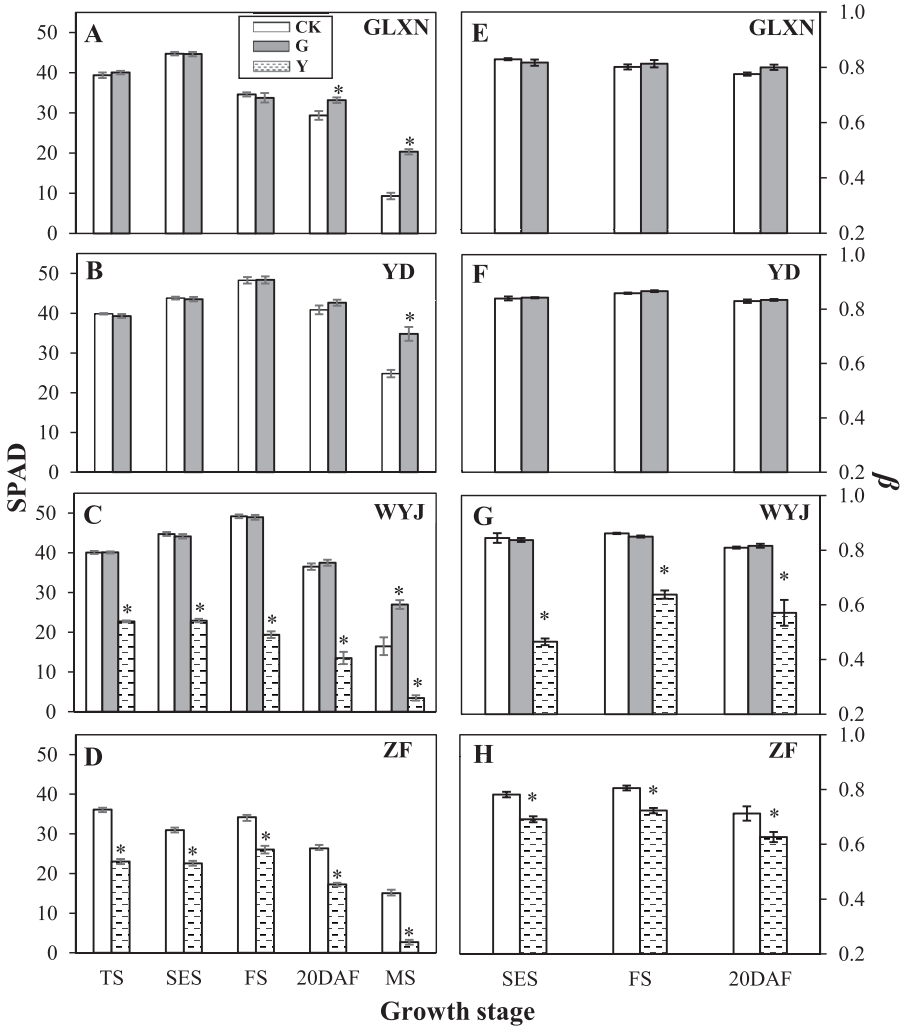

Fig. 1. Changes of leaf SPAD (A–D) and leaf light absorptance (β, E-H) for four default rice genotypes (CK) and their greener-leaf variants (G) or yellower-leaf variants (Y) at different stages: tillering stage (TS), stem-elongating stage (SES), flowering stage (FS), 20 d after flowering (20DAF), and maturity stage (MS). Vertical bars ± standard errors represent the means of four replicates. The asterisks (*) indicate statistical significance at the $P < 0.05$ level between variant genotype and its default genotype within a given stage. Genotype-background abbreviations: GLXN, cv. Guanglingxiangnuo; YD, cv. Yandao 8; WYJ, cv. Wuyunjing 3; and ZF, cv. Zhefu 802.

O_2), given that values of these Rubisco parameters are believed to be conserved among C_3 species (von Caemmerer, 2000).

2.5. Quantifying energy levels for non-photochemical quenching

The commonly used fluorescence parameter NPQ (NPQ = $Fm/F'm-1$) can indicate a magnitude of thermal dissipation; however, this parameter can go up to high values of >1.0, which is not conducive to quantifying the relative share of energy by NPQ vs photochemistry (Hendrickson et al., 2004). Here, to better quantify the relative energy loss primarily via NPQ, we propose an alternative way as described below, using the measured Φ_2. If there was no thermal dissipation, one would expect that the total PSII electron flux (J_2) increases linearly with increasing absorbed irradiance (I_{abs}), and then J_2 would be expressed as $\rho_2 I_{abs}\Phi_{2LL}$, where ρ_2 is the partitioning factor of I_{abs} to PSII, and combined $\rho_2\Phi_{2LL}$ may also be denoted as the PSII electron transport efficiency based on light absorbed by both photosystems (α_{2LL}). As Φ_2 decreases with increasing I_{abs}, the difference between $\rho_2 I_{abs}\Phi_{2LL}$ and $\rho_2 I_{abs}\Phi_2$ must be the electron-equivalent flux of energy dissipated as NPQ (J_{NPQ}) (see Fig. S1a). Then the fraction of the energy that is lost via NPQ (F_{npq}) can be expressed relative to $\rho_2 I_{abs}\Phi_{2LL}$, which can be simplified to:

$$F_{npq} = \frac{J_{NPQ}}{\rho_2 I_{abs}\Phi_{2LL}} = \frac{\rho_2 I_{abs}\Phi_{2LL} - \rho_2 I_{abs}\Phi_2}{\rho_2 I_{abs}\Phi_{2LL}} = 1 - \frac{\Phi_2}{\Phi_{2LL}} \quad (5)$$

Unlike the fluorescence parameter NPQ, values of F_{npq} are within the range between 0 and 1. Similar to the method of Hendrickson et al. (2004), Eqn (5) quantifies the relative partitioning of excitation energy between photochemistry and thermal dissipation. The third (but small) share of energy lost by fluorescence, which is shown to be quite constant (ca. 0.25) across light levels (Hendrickson et al., 2004), is only implicitly accounted for via parameter Φ_{2LL} in Eqn (5), whose value was ca. 0.70–0.75 for our genotypes (Table 3). Because Eqn (5) uses the strict limiting light level as a departure point (Fig. S1a), it does not require F_m (the dark-adapted maximum fluorescence yield) to calculate F_{npq}; but, as shown later, the obtained F_{npq} gives similar patterns of response to the light level as NPQ.

It is useful to calculate the incident-irradiance level at which the energy flux lost via NPQ (J_{NPQ}) is equal to total PSII electron flux (J_2), i.e. the point where 50% of the absorbed light energy is consumed by PSII electron transport and NPQ each (Fig. S1b). We denote this point of incident-irradiance as I_{50} and the corresponding J_2 as J_{50}. Values of I_{50} and J_{50} are commonly solved from fitting additional empirical quadratic equations for both J_{NPQ} and PSII electron flux (Meacham et al., 2017). We found introducing additional empirical equations unnecessary, and I_{50} and J_{50} can be calculated from earlier estimated parameter values of Eqn (A3b) of the 'FvCB model':

$$\begin{cases} I_{50} = \dfrac{2J_{max}}{(2-\theta)\kappa_{2LL}} \\ J_{50} = \dfrac{J_{max}}{2-\theta} \end{cases} \quad (6)$$

The derivation of Eqn (6) is given in Supplementary Appendix B.

2.6. Estimation of quantum yield of leaf photosynthesis

The quantum yield for leaf CO_2 assimilation under limiting light conditions (Φ_{CO2LL}) was calculated on the basis of either incident or absorbed irradiance, according to the method described by Yin et al. (2014):

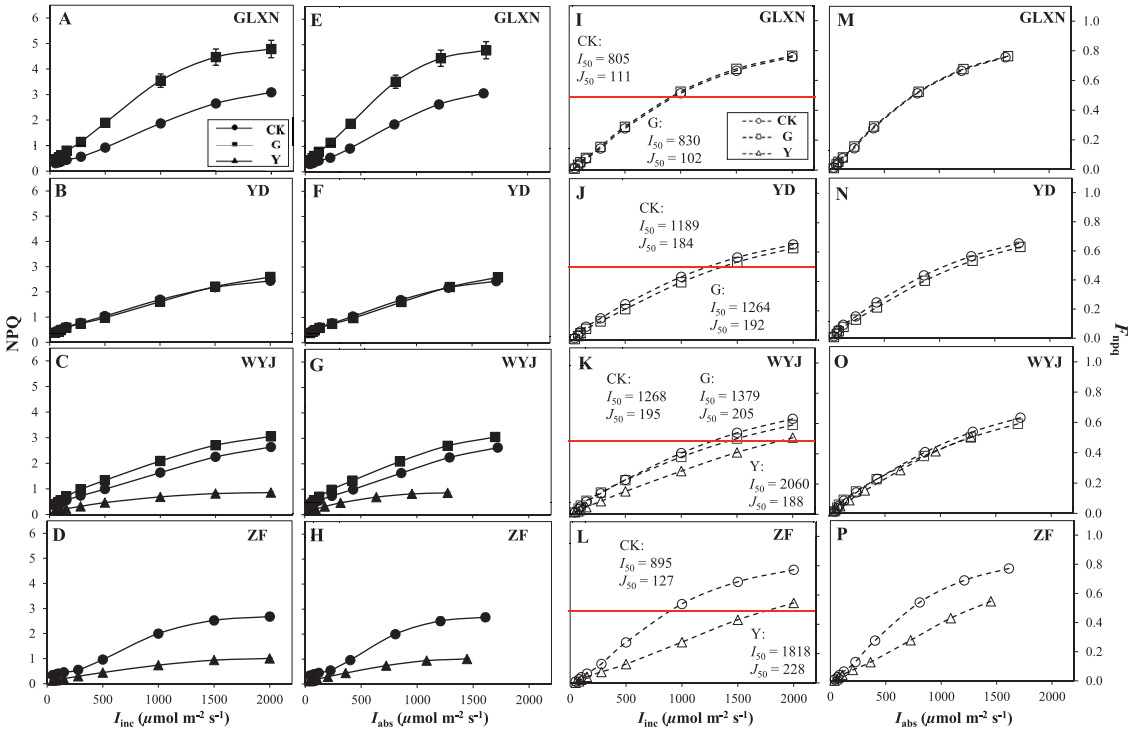

Fig. 2. The response curves of NPQ (A–H) and F_{npq} (I–P) for four default rice genotypes (CK, circle) and their greener-leaf variants (G, square) or yellower-leaf variants (Y, triangle) at flowering stage based on incident light (I_{inc}) or absorbed light (I_{abs}). Each data point from the NPQ response curve (represented by filled symbols with continuous curves) is the mean value of three or four replicates (± standard errors). The curves of F_{npq} (represented by open symbols with dotted curves) were drawn using Eqn (5). The red horizontal line in panels I–L is the line that F_{npq} = 0.5, whose intersection points with the curves correspond to the incident light level (I_{50}), at which the absorbed light energy is equally used between NPQ and driving electron transport, i.e. $J_2 = J_{NPQ}$ (see Fig. S1b). Values of I_{50} (μmol m^{-2} s^{-1}) and its corresponding potential e^- transport rate J_{50} (μmol m^{-2} s^{-1}), calculated by Eqn (6), are given. Genotype-background abbreviations: GLXN, cv. Guanglingxiangnuo; YD, cv. Yandao 8; WYJ, cv. Wuyunjing 3; and ZF, cv. Zhefu 802.

$$\begin{cases} \Phi_{CO2LL(inc)} = s' \Phi_{2LL}/4 \\ \Phi_{CO2LL(abs)} = s' \Phi_{2LL}/(4\beta) \end{cases} \quad (7)$$

where Φ_{2LL} is Φ_2 at the irradiances approaching to zero, which can be estimated as earlier described, and s' is the linear slope factor of regressing A against ($\Phi_2 I_{inc}/4$). Mathematically s' is equal to $s[(C_c - \Gamma_*)/(C_c + 2\Gamma_*)]$ (Yin et al., 2014). For non-photorespiratory conditions, parameter s' is equal to the above-mentioned calibration factor s. This method overcomes the error of the conventional quantum yield estimating method that assumes a constant Φ_2 over the irradiance range used to estimate Φ_{CO2LL}.

2.7. Statistical analyses and curve fitting

Simple linear regressions were conducted using Microsoft Excel. Nonlinear regressions were performed using the Gauss method in PROC NLIN of SAS (SAS Institute Inc., Cary, NC, USA). Significance of differences was assessed based on one-way analysis of variance (ANOVA) and least significant difference (LSD) test. The photosynthesis parameters were estimated by using pooled data of three or four replicates from gas exchange and chlorophyll fluorescence, which in fact are close to the mean of replicated estimates but have better statistical predictions of all data points than the mean. Therefore, no significant-difference tests were applied in these estimated photosynthesis parameters (Table 3).

3. Results

3.1. Altered leaf chlorophyll content of variant genotypes

In the field experiment, we measured both [CHL] and SPAD for all genotypes, which were positively correlated ($R^2 = 0.99$) (Fig. S2a). Data obtained from the greenhouse experiment showed that leaf absorptance (β) was hyperbolically related to SPAD (Fig. S2b), in a shape similar to the function that Evans (1996) described for the correlation between β and [CHL]. These observations together suggest that SPAD values of leaves can reflect the trend of [CHL]. Moreover, the similar trends of SPAD (Fig. S2c) and of A_{max} (Fig. S3) in the greenhouse experiment and the field experiment indicated that the character of altered [CHL] had been well maintained across the environments. Visual images of leaf colour differences among genotypes from the greenhouse experiment can be found in Fig. S4.

For the greenhouse experiment, there were no significant differences between stay-green genotype variants (G) and their default control genotypes (CK) in terms of SPAD value and β, except for the former at post-flowering stages when the stay-green genotypes began to exhibit the delayed senescence of leaves (Fig. 1A–D). For yellow-leaf genotype variants (Y), however, a significant drop in SPAD was observed with, on average, 57.4% and 28.5% decrease for WYJ and ZF background, respectively, across stages. Similar patterns were shown in β between Y variants and their CK genotypes (Fig. 1E–H); β declined much more in WYJ-Y than in ZF-Y across the stages.

3.2. Proportions of energy for non-photochemical quenching

The two G genotypes showed higher NPQ than their CK genotypes, particularly in GLXN based on either I_{inc} or I_{abs} (Fig. 2A–H). Fig. 2I-P shows values of F_{npq} calculated using Eqn (5). The response curve of F_{npq} for each G genotype almost coincided with its CK counterpart (Fig. 2I–K). Like their NPQ values, values of F_{npq} were lower in Y genotypes than in other genotypes, when plotted against I_{inc}. When plotted against I_{abs}, curves of F_{npq} for three genotypes from the WYJ background almost overlapped, but the Y genotype from the ZF background still had lower F_{npq} than its CK counterpart (Fig. 2O–P).

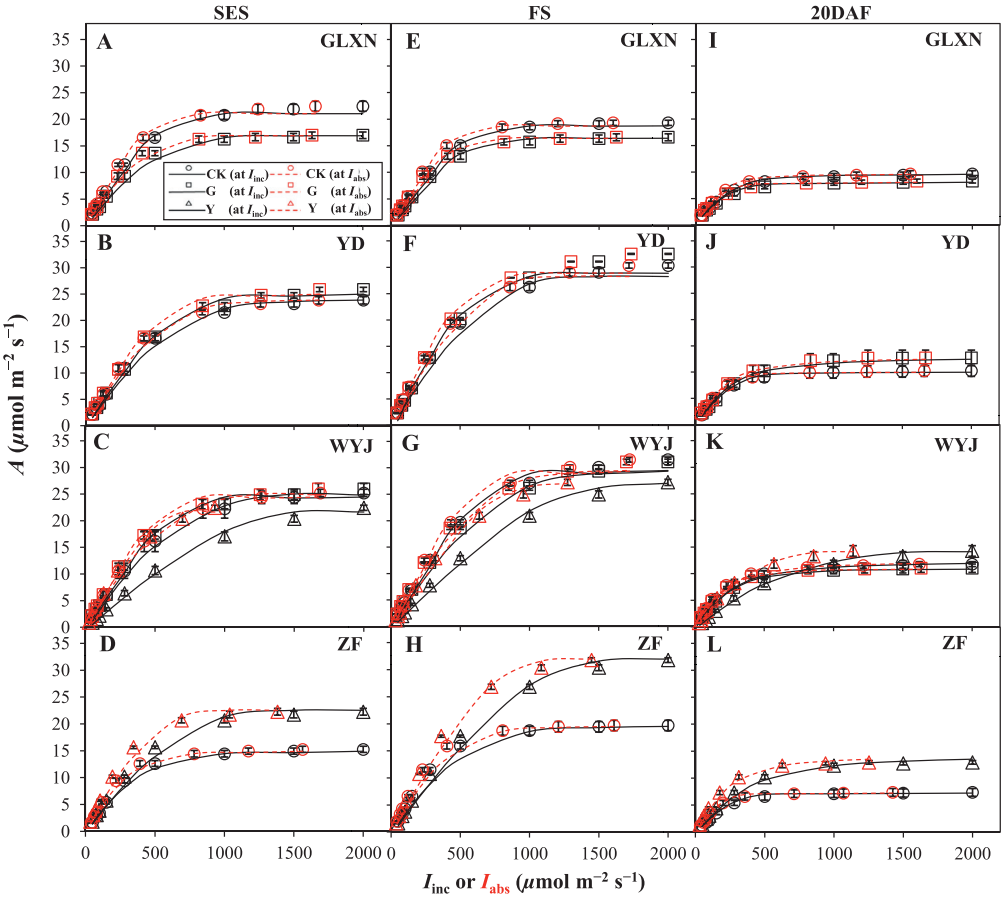

Fig. 3. The response curves of photosynthesis (A) for four default rice genotypes (CK, circle) and their greener-leaf variants (G, square) or yellower-leaf variants (Y, triangle) (GLXN: A, E, I; YD: B, F, J; WYJ: C, G, K; ZF: D, H, L) at stem-elongating stage (SES, A-D), flowering stage (FS, E-H), and 20 d after flowering (20DAF, I-L) based on I_{inc} (black symbols and continuous curves) or I_{abs} (red symbols and dotted curves) under CO_2 concentration of 400 μmol mol^{-1}. Data (represented by different symbols) are shown as means of three or four replicates (± standard errors) for each genotype. The curves were drawn using fitted parameter values of Eqn (4). Genotype-background abbreviations: GLXN, cv. Guanglingxiangnuo; YD, cv. Yandao 8; WYJ, cv. Wuyunjing 3; and ZF, cv. Zhefu 802.

Fig. 2I-L also describes an equilibrium state of dissipation and photochemical energy utilisation at the flowering stage, calculated by Eqn (6). There were variations in I_{50} or J_{50}, beyond which J_{NPQ} started to exceed J_2 and to become dominant. Compared with the slight differences between G and CK, there were more significant differences between Y and CK genotypes. The I_{50} values increased significantly in both Y materials, compared with their CK. For J_{50}, the Y genotypes of two backgrounds showed different trends relative to their CK counterparts. There was a slight decrease (4%) in J_{50} of WYJ-Y whereas ZF-Y showed a large increase (80%) in J_{50}.

3.3. Photosynthetic characteristics derived from response curves

Light response curves of A measured in the greenhouse experiment for different stages are given in Fig. 3. Since the stay-green variants did not yet begin to manifest themselves, there were slight differences in A between G and CK genotypes. Under saturated light intensity, GLXN showed a slightly lower A in G than in CK while YD had slightly increased A in G over CK genotypes. By comparison, a completely different effect of Y variants was noted between WYJ and ZF backgrounds. A in WYJ-Y was much lower than that in WYJ-CK under high I_{inc}, whereas the difference was opposite between ZF-Y and ZF-CK. If A is plotted against I_{abs}, the curves for WYJ-Y and WYJ-CK almost overlapped while the advantage of ZF-Y under high light levels was maintained. This indicated that the difference between WYJ-Y and WYJ-CK can predominantly be attributed to the difference in β, whereas for the ZF background, the effect of the Y variant involved additional mechanisms. A similar difference between variant genotype and its default genotype was observed from their CO_2 response curves (Fig. 4).

The estimated photosynthetic parameters for these genotypes at three stages are shown in Table 3. There were no significant differences between variants and their default genotypes at any stage for parameter R_d ($P > 0.05$). There were negligible differences in the efficiency of converting irradiance into electron transport (κ_{2LL}) and photosynthetic capacity parameters (i.e. J_{max}, V_{cmax}, and T_p) for G genotypes, but larger differences were found between Y and CK genotypes. Compared with the CK genotypes, parameters Φ_{2LL} and s were lower in Y materials, and as a result, κ_{2LL} derived from Eqn (2) decreased by ca. 40% and 10% in WYJ-Y and ZF-Y, respectively. The WYJ-Y demonstrated no apparent change in J_{max} and V_{cmax} but a decline occurred in T_p at stem-elongating and flowering stages. However, for the ZF-Y genotype, simultaneous improvements in J_{max}, V_{cmax}, and T_p were observed with an average increase by 61%, 69%, and 26%, respectively, across the three stages. In addition, the apparent carboxylation efficiency (CE) of ZF-Y also increased significantly (Fig. 4), suggesting a possibly improved Rubisco activity.

Stomatal conductance (g_s) was little affected in G variants except for some variations in GLXN at stem-elongating stage, while a greater impact was observed in Y variants due to significantly increased g_s relative to the CK (Table 4). Both GLXN-G and WYJ-Y had a significantly lower mesophyll conductance (g_m) at stem-elongating and flowering stages, but a higher g_m was observed in YD-G. Notably, ZF-Y maintained the higher g_m at all stages.

3.4. Photosynthetic nitrogen distribution pattern

Since SPAD increased proportionally with the increase of [CHL] (Fig. S2a), we calculated the ratio of each of the earlier estimated photosynthesis parameters to the SPAD value as indicators of these parameters per unit [CHL] (Table S1). A large increase in the ratios was found in both Y genotypes at all stages, suggesting a change in the relative N investment between light-harvesting complex and other photosynthetic proteins.

The leaf N partitioning to photosynthetic proteins was further assessed with the relative abundance of photosynthetic proteins as shown in a heatmap via a proteomic enrichment analysis (Fig. 5). For the stay-green case, the relative expression of most photosynthetic proteins in the

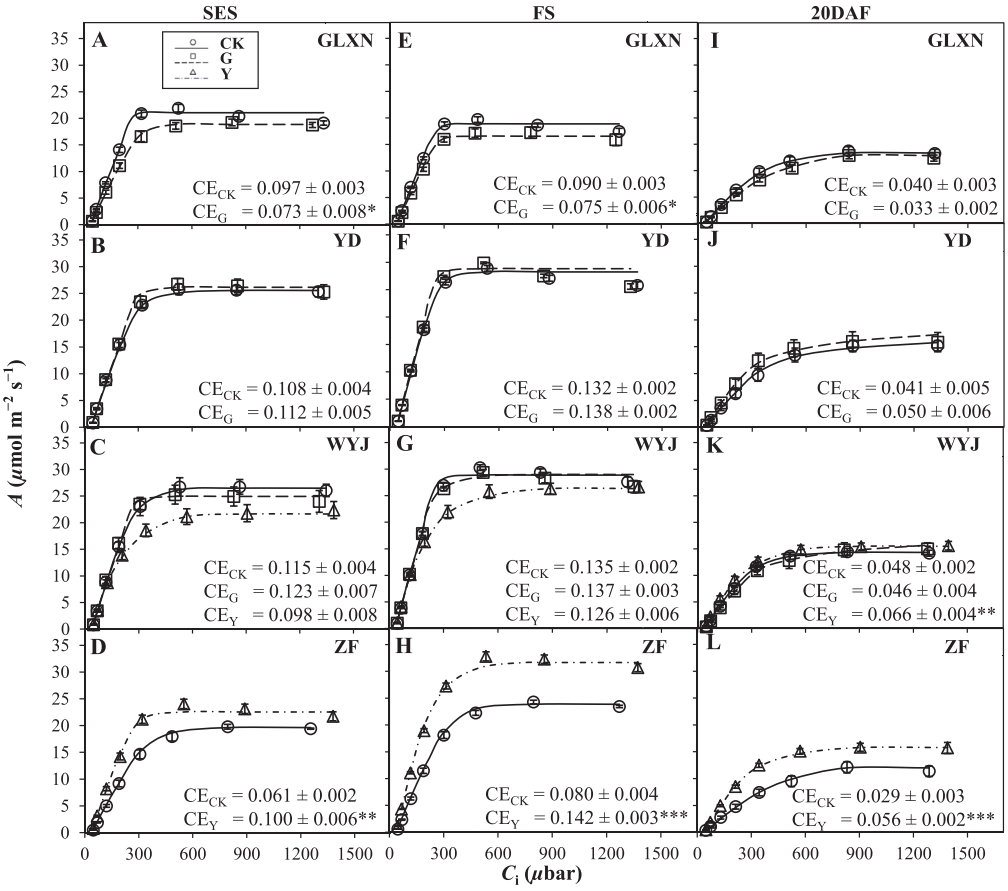

Fig. 4. The CO_2 response curves for four default rice genotypes (CK, circle) and their greener-leaf variants (G, square) or yellower-leaf variants (Y, triangle) (GLXN: A, E, I; YD: B, F, J; WYJ: C, G, K; ZF: D, H, L) at stem-elongating stage (SES, A-D), flowering stage (FS, E-H), and 20 d after flowering (20DAF, I-L) under light intensity of 1,000 μmol m^{-2} s^{-1}. Apparent carboxylation efficiency (CE, mol m^{-2} s^{-1} bar^{-1}) was calculated as the initial slope of the CO_2 response curve as listed in each panel. The word "apparent" is used here because the initial slope also includes a component of mesophyll conductance (see Fig. 6). A significant difference between variant genotype and its default genotype in CE is shown by asterisks: *$P < 0.05$, **$P < 0.01$ and ***$P < 0.001$. Data (represented by different symbols) are shown as means of three or four replicates (± standard errors) for each genotype. The curves were drawn from using fitted parameter values of Eqn (4). Genotype-background abbreviations: GLXN, cv. Guanglingxiangnuo; YD, cv. Yandao 8; WYJ, cv. Wuyunjing 3; and ZF, cv. Zhefu 802.

Table 4
CO_2 diffusion parameters, specific leaf area (SLA, $m^2\ kg^{-1}$), specific leaf nitrogen (SLN, g N m^{-2}), and leaf photosynthetic nitrogen-use efficiency (PNUE, μmol CO_2 g^{-1} N s^{-1}) for four default rice genotypes (CK) and their greener-leaf variants (G) or yellower-leaf variants (Y) at three stages.

Stage	Background	Genotype	g_s[a]	g_m[a]	SLA	SLN	PNUE[b]
Stem-elongating	GLXN	CK	0.370 (0.028)	0.161 (0.006)	22.9 (0.20)	1.15 (0.02)	24.3 (0.76)
		G	0.260 (0.015)*	0.125 (0.005)*	23.5 (0.35)	1.01 (0.03)*	21.7 (0.84)*
	YD	CK	0.401 (0.033)	0.169 (0.006)	26.4 (0.53)	1.37 (0.04)	20.8 (0.64)
		G	0.367 (0.030)	0.192 (0.007)*	25.9 (0.74)	1.36 (0.08)	23.2 (1.86)
	WYJ	CK	0.334 (0.006)	0.190 (0.007)	27.1 (1.24)	1.48 (0.06)	20.3 (1.21)
		G	0.346 (0.030)	0.195 (0.007)	26.4 (1.17)	1.27 (0.05)*	24.9 (1.20)*
		Y	0.433 (0.045)*	0.155 (0.005)*	30.8 (0.28)*	1.40 (0.03)	19.2 (0.79)
	ZF	CK	0.208 (0.023)	0.113 (0.004)	21.7 (0.72)	0.92 (0.03)	21.5 (0.79)
		Y	0.442 (0.032)*	0.154 (0.007)*	28.7 (0.99)*	1.01 (0.06)	29.1 (1.73)*
Flowering	GLXN	CK	0.227 (0.015)	0.138 (0.003)	21.9 (0.32)	1.11 (0.03)	21.9 (0.47)
		G	0.203 (0.015)	0.117 (0.005)*	22.2 (0.43)	0.98 (0.05)*	22.2 (0.71)
	YD	CK	0.516 (0.021)	0.204 (0.005)	23.4 (0.36)	1.66 (0.05)	21.3 (1.00)
		G	0.508 (0.012)	0.227 (0.001)*	22.5 (0.54)	1.65 (0.02)	22.9 (0.43)
	WYJ	CK	0.421 (0.031)	0.224 (0.002)	22.5 (0.65)	1.71 (0.05)	21.4 (1.00)
		G	0.451 (0.020)	0.218 (0.003)	23.3 (0.46)	1.74 (0.01)	20.6 (0.33)
		Y	0.529 (0.024)*	0.176 (0.004)*	26.2 (0.46)*	1.54 (0.06)*	20.8 (1.07)
	ZF	CK	0.299 (0.019)	0.132 (0.007)	21.3 (0.39)	1.05 (0.03)	21.3 (0.63)
		Y	0.583 (0.021)*	0.214 (0.005)*	24.0 (0.64)*	1.57 (0.02)*	23.6 (0.36)*
20 d after flowering	GLXN	CK	0.191 (0.023)	0.073 (0.006)	22.6 (0.37)	0.69 (0.05)	21.0 (0.84)
		G	0.168 (0.009)	0.062 (0.003)	21.8 (0.36)	0.72 (0.02)	17.0 (0.80)*
	YD	CK	0.188 (0.018)	0.079 (0.008)	27.4 (0.67)	0.86 (0.05)	16.4 (1.81)
		G	0.226 (0.027)	0.100 (0.013)	26.7 (0.55)	0.92 (0.03)	18.3 (1.49)
	WYJ	CK	0.190 (0.015)	0.092 (0.005)	27.2 (0.52)	0.81 (0.03)	20.3 (0.56)
		G	0.209 (0.033)	0.083 (0.006)	28.5 (1.15)	0.77 (0.04)	20.5 (1.58)
		Y	0.284 (0.025)*	0.110 (0.005)	28.1 (0.93)	1.27 (0.04)*	13.8 (1.40)*
	ZF	CK	0.150 (0.017)	0.056 (0.006)	20.4 (0.55)	0.58 (0.03)	19.9 (2.00)
		Y	0.375 (0.061)*	0.094 (0.002)*	26.4 (0.99)*	0.70 (0.01)*	27.3 (1.17)*

Data (mean with standard error of three or four replicates in brackets) show the variant genotype significantly different from those of its default genotype (*$P < 0.05$).

[a] G_s refers to stomatal conductance for CO_2 diffusion, while g_m was derived from the fitted model, both for a light intensity of 2,000 μmol m^{-2} s^{-1} and a CO_2 concentration of 400 μmol mol^{-1}.

[b] Leaf photosynthetic nitrogen-use efficiency (PNUE) was defined as: PNUE $= \frac{A_{max}}{SLN - n_b}$, where A_{max} is the maximum net photosynthesis rate at a light intensity of 2,000 μmol m^{-2} s^{-1} and a CO_2 concentration of 400 μmol mol^{-1}, and n_b represents a base leaf nitrogen content with an estimate of 0.23 g N m^{-2} for n_b (see Fig. 7).

YD background was slightly increased while an opposite trend was observed in GLXN background. There was almost no difference of these photosynthetic proteins in WYJ-G compared with its CK, except for a downregulation in Lhca1-4 involved in Photosystem I (PSI). For the yellow-leaf case, both Y genotypes showed a lower relative abundance of light-harvesting proteins (Lhcb1-6 and Lhca1-4 from PSII and PSI, respectively), with a much more significant decline in WYJ than in ZF. In addition, other photosynthetic proteins did not change much in WYJ-Y. However, ZF-Y notably increased the relative abundance of Cytochrome b_6/f complex (Cyt b_6/f) and Rubisco related proteins.

Following the proteomic data format, we calculated the relative changes of Rubisco carboxylation activity from the CE derived from A-C_i curves. There was a positive correlation between relative Rubisco content from proteomic data and relative Rubisco carboxylation activity from gas exchange data (Fig. 6).

3.5. Leaf morphological traits and photosynthetic nitrogen-use efficiency

The SLA was little affected in G variants, but was significantly higher in Y variants than in the CK (Table 4). Similarly, there was no remarkable difference SLN between G and CK (Table 4). No consistent change in SLN across stages was found in WYJ-Y compared with its CK, while SLN of ZF-Y was always higher than that of CK at three stages with a significant effect shown after flowering. The variation in SLN, either across genotypes or across stages, was positively correlated with the A_{max} value ($R^2 = 0.89$) as shown in Fig. 7 that gives an estimate of base leaf N of n_b = 0.23 g N m^{-2}. Based on this n_b, we calculated the values for PNUE at a light intensity of 2,000 μmol m^{-2} s^{-1} and a CO_2 level of 400 μmol mol^{-1}. As expected from the linear relation between A_{max} and SLN, most genotypes did not show a significant difference in PNUE, except for a decrease in GLXN-G (at stem-elongating and grain-filling stages) and WYJ-Y (at grain-filling stage) compared with their CK. Conversely, despite some increase in SLN, the PNUE of ZF-Y had still been improved significantly at all stages.

4. Discussion

4.1. Negligible impact of stay-green variants prior to the maturity stage

The G genotypes presented delays in chlorophyll catabolism only when the plants were approaching maturity, as shown by the SPAD values (Fig. 1A–D). Across all the earlier stages, there were negligible differences between G and CK genotypes in leaf absorptance β (Fig. 1E–H), photosynthetic capacity (i.e. J_{max}, V_{cmax}, and T_p, Table 3), and even PNUE (Table 4). Such a result was also found in stay-green genotypes of other species, like wheat (Chen et al., 2010) and maize (Zheng et al., 2009). These results are not surprising given that stay-green traits are mainly meant to sustain leaf photosynthetic competence during later grain filling (Borrell et al., 2014; Gregersen et al., 2013). It is worthwhile to study whether the stay-green traits indeed delay declines in photosynthesis or just are cosmetic phenotypes when approaching maturity.

4.2. Impact of restrained light-absorptance ability in yellow-leaf variants

Given the hyperbolic relation between β and SPAD (Fig. S2), the Y variants impacted leaf light-absorptance ability throughout the entire crop cycle with decreased SPAD values (Fig. 1A–D) and light-harvesting proteins (Fig. 5). Rotasperti et al. (2022) reported that the barley mutant with decreased leaf SPAD and truncated antenna size increased photosynthetic efficiency but this is not a universal case. Excessive suppression of β would be detrimental for plants in limiting-light environments (Ort et al., 2011). In our study, the average decline in leaf β of WYJ-Y was triple that of ZF-Y across the three stages, relative to their CK (Fig. 1G and H). Overly reduced β values in WYJ-Y led to reduced photosynthetic parameters (s and

Uniprot ID	GLXN	YD	WYJ		ZF		
	G-vs-CK	G-vs-CK	G-vs-CK	Y-vs-CK	Y-vs-CK		
P12331	-0.2420	0.5768	0.2456	-2.0001	-1.0766	Lhcb1	Photosystem II
Q10HD0	-0.7174	0.3301	0.1291	-2.8031	-0.4196	Lhcb2	
A3BL59	-0.8704	0.5867	-0.0657	-3.1804	-0.7351	Lhcb3	
Q0D5I4	-0.1174	0.6355	0.0446	-2.7484	-1.0470	Lhcb4	
A3CA44	-0.6874	0.4175	0.1217	-1.6199	-0.3082	Lhcb5	
Q0JCQ4	-0.8256	0.3863	-0.1261	-2.3349	-0.2060	Lhcb6	
P0C434	-0.0990	0.6497	-0.2602	-0.9274	-0.5135	PsbA	
P0C437	-0.8898	1.0468	-0.2160	-0.2333	0.2750	PsbD	
P0C364	-0.0270	0.5830	-0.0766	-0.6974	-0.4527	PsbB	
A0A0P0WWB9	-2.1490	0.3844	-1.9131	-2.8264	-0.4724	Lhca1	Photosystem I
A0A0P0X812	-1.0799	0.1334	-1.7069	-3.7381	-0.6059	Lhca2	
A3A460	-2.2421	0.3073	-1.6763	-3.3090	-0.6427	Lhca3	
A3BTG2	NA	0.0849	-2.8658	-4.1452	-0.4813	Lhca4	
P0C355	0.2214	0.7943	0.0285	-1.7501	-1.5910	PsaA	
P0C358	-1.8618	1.2141	-0.2188	-1.4393	-0.2533	PsaB	
P0C389	-0.0149	0.2230	-0.0905	-0.6174	0.2763	PetA	Cytochrome b6/f complex
P12123	-1.0687	0.3261	-0.0517	-0.5080	0.6134	PetB	
Q69S39	-1.5072	-0.2666	-0.5107	-0.2797	1.5697	PetC	
P12124	-1.5589	0.5868	-0.2746	-0.2008	0.4788	PQ	Photosynthetic electron transport
Q0DFC9	0.0297	0.1545	-0.6023	-1.1007	0.0060	PC	
A0A5S6R7Q0	0.4484	-0.6733	0.6449	0.0046	-0.7291	Fd	
P41344	0.2106	0.1300	0.0504	-0.2456	-0.1499	FNR1	
Q6ZFJ3	0.1311	-0.2645	0.0091	-0.5180	-0.2987	FNR2	
P12085	0.0960	-0.0231	-0.1747	-0.5486	-0.3247	beta	F-type ATPase
P0C2Z6	0.0995	0.5413	-0.0233	-0.4137	-0.6764	alpha	
Q0D641	0.0430	0.6261	0.0337	-0.3134	-0.8762	gamma	
Q6Z8K7	-0.7172	-0.5954	-0.8154	0.0702	0.7837	delta	
P0C2Z3	-0.1321	0.1435	-0.2142	-0.3450	0.1460	epsilon	
P0C2Z0	-0.8140	1.0271	-0.5358	-0.8163	0.2693	b	
P0C512	0.1499	0.2331	0.0127	-0.3252	-0.0940	rbcL	Rubisco related proteins
Q0DB64	2.9939	2.3313	0.2112	-0.5387	3.2524	rbcL	
Q0IPF7	-0.1394	-0.2988	-0.4041	0.0232	0.0000	rbcL	
Q339G9	0.2065	0.6013	0.8805	-0.0370	0.1494	rbcL	
P18566	-0.8209	0.7299	-0.2722	0.0114	1.1706	rbcS	
Q2QTK0	-1.4176	0.5931	-0.8418	-0.5177	1.7170	rbcS	
P93431	-0.2906	-0.3306	-0.1482	-0.4034	0.2521	RCA	
H2KVX3	-0.4159	-0.0271	-0.4086	-0.4122	0.5939	RCA	
A2ZVV8	-0.1979	0.5308	-0.2663	0.4069	0.6330	CA	

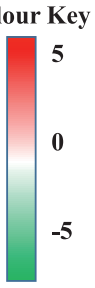

Fig. 5. Heat map of proteins of photosynthesis in four default rice genotypes (CK) and their greener-leaf variants (G) or yellower-leaf variants (Y) at flowering stage. Each column represents a comparison group (i.e. variant genotype vs default genotype) and each row represents a protein with its uniprot ID listed on the left. The Log_2(Foldchange) value of the protein was shown in a heat map in different colours, with red representing up-regulation and green representing down-regulation. Significant difference existed when log_2(Foldchange) > 1. NA means the protein of sample was not detected. Protein abbreviations on the right: Lhcb1-6, chlorophyll *a-b* binding proteins in the light-harvesting complex of Photosystem II (LHCII); PsbA, D1 protein of Photosystem II; PsbD, D2 protein of Photosystem II; PsbB, cp47 reaction centre protein of Photosystem II; Lhca1-4, chlorophyll *a-b* binding proteins in the light-harvesting complex of Photosystem I (LHCI); PsaA, P700 chlorophyll a apoprotein A1 of Photosystem I; PsaB, P700 chlorophyll a apoprotein A2 of Photosystem I; PetA-C, components of the cytochrome b_6/f complex (cyt b_6/f); PQ, NAD(P)H-quinone oxidoreductase subunit; PC, Plastocyanin; Fd, Ferredoxin; FNR1-2, Ferredoxin-NADP reductase; beta, alpha, gamma, delta, epsilon, and b are ATP synthase subunits; rbcL, Ribulose bisphosphate carboxylase large chain; rbcS, Ribulose bisphosphate carboxylase small chain; RCA, Rubisco activase; and CA, carbonic anhydrase. Genotype-background abbreviations: GLXN, cv. Guanglingxiangnuo; YD, cv. Yandao 8; WYJ, cv. Wuyunjing 3; and ZF, cv. Zhefu 802.

Φ_{2LL}), which strongly decreased irradiance-to-electron conversion efficiency (i.e. κ_{2LL}, Table 3) and the quantum yield of photosynthesis (Table S2). By contrast, ZF-Y was less affected in this respect. Besides, the photosynthetic difference between Y and CK in the WYJ background was mainly due to reduced β given the overlapping light response curves based on I_{abs} (Fig. 3) and similar photosynthetic capacity parameters (Table 3) when excluding the effects of leaf SLN. In addition, modifying leaf [CHL] changed not only light harvesting and resultant physiology, but also leaf morphology, as shown by the significantly increased SLA of Y variants (Table 4). This impact of restrained β on SLA could be analogous to the commonly observed thin leaves when plants grow under low-light conditions (Evans and Poorter, 2001). Xiao et al. (2016) also showed that the leaf anatomical features, especially those controlling the light distribution inside a leaf, can influence the β value of a leaf.

4.3. Shift in balance between thermal dissipation and photochemical energy utilisation

Similar to previous reports (Gu et al., 2017a,b; Li et al., 2013), our results (Fig. 2A–H) for differences in either G or Y variants relative to CK were observed for NPQ using conventional calculation, i.e. NPQ = $Fm/Fm-1$, indicating the potential of thermal dissipation for variants was altered. However, as mentioned earlier, these calculated NPQ values can go beyond 1.0, which is not handy to evaluate the relative consumption of absorbed energy between NPQ and photochemistry. So, derived from the actual photochemical efficiency of PSII, F_{npq} is proposed (see Eqn (5)) to describe the actual relative energy loss due to NPQ under fluctuating light environment (Fig. 2I-P). The method follows a similar consideration as Hendrickson et al. (2004) discussed – the relative energy loss via NPQ is presented by a value between 0 and 1, and the absolute energy loss primarily via NPQ was presented as an electron-equivalent flux (J_{NPQ}), which competed with the total PSII electron flux (J_2) (see Fig. S1b). With this method, we found that the difference in F_{npq} between G and CK almost disappeared based on either I_{inc} or I_{abs}, indicating the distribution pattern of absorbed energy between J_2 and J_{NPQ} was not changed by G variants. The same result was found for WYJ-Y although a small deviation from the F_{npq} curve between WYJ-Y and WYJ-CK under I_{inc} was caused by β. In contrast, ZF-Y had a lower F_{npq} compared with its CK, suggesting an increased energy demand for photosynthetic metabolisms.

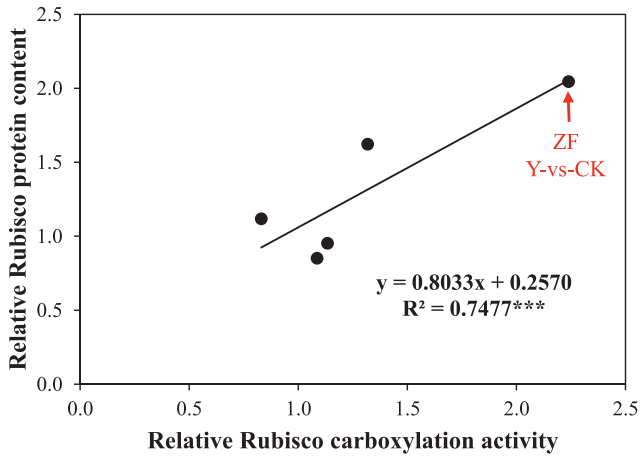

Fig. 6. Relationship between relative Rubisco protein content and relative Rubisco carboxylation activity. The relative Rubisco protein content was obtained by averaging the back-calculated relative contents (from proteomics data in Fig. 5 for $\log_2$(Foldchange)) of all the subunits of Rubisco protein from each comparison group (i.e. variant genotype vs default genotype). The relative Rubisco carboxylation activity was calculated from the residual Rubisco carboxylation resistance, which is $(1/CE - 1/g_m)$ according to the method described in Yin et al. (2009), where CE is carboxylation efficiency (mol m^{-2} s^{-1} bar^{-1}) calculated as the initial slope of the photosynthetic CO_2 response curve (see Fig. 4), and g_m is mesophyll diffusion conductance (mol m^{-2} s^{-1} bar^{-1}) calculated based on Eqn (4) at C_i*, the C_i-based CO_2 compensation point in the absence of R_d. Then the relative Rubisco carboxylation activity shown in the X-axis can be calculated as the ratio of $[1/(1/CE - 1/g_m)]$ of the variant genotype to that of its default genotype. Linear regression was fitted for overall data with its significance of correlation shown by asterisks: ***P < 0.001.

The intersection point (I_{50}, J_{50}) of J_2 and J_{NPQ} curves represents a balance of coordination between photochemical reactions and the thermal dissipation (Gilmore et al., 1996). Based on the 'FvCB model', Eqn (6) was derived from estimated photosynthetic parameters, which not only avoids additional empirical equations applied in the analysis of Meacham et al. (2017), but also prevents an uncertain assumption made by Hendrickson et al. (2004) and Meacham et al. (2017) that the proportion of I_{abs} partitioned to PSII is 0.5. Our formulae for the balance point (I_{50}, J_{50}) could be used for screening genotypes with greater potential for improved light use efficiency. Through calculating this balance point, we examined the genotypic variation after modifying [CHL]. Both I_{50} were much higher in Y than in CK genotypes (Fig. 2K-L), suggesting an enhanced high-light tolerance in Y genotypes. But only ZF-Y showed an increase in J_{50}, indicating an elevated energy utilisation efficiency. Our result suggests that manipulation of leaf [CHL] alone could exert a certain influence on the light energy distribution between J_2 and J_{NPQ} by adjusting β, but it does not necessarily result in an improved energy use competence in leaves. Therefore, we concluded that only by improving the capacity of photochemical energy utilisation can the share of light energy allocated to NPQ be substantially reduced.

4.4. *Dependence of nitrogen distribution strategy on genetic background*

The positive correlation between SLN and A_{max} (Fig. 7) indicated that photosynthesis was mainly determined by leaf N content across either genotypes or stages, but when SLN was similar, variation in A_{max} among the same genetic background can be explained by different N investment patterns. There was a higher 'work efficiency' per unit [CHL] in Y variants than in default genotypes (Table S1). Among the two genetic backgrounds having the Y-variants, only the Y genotype from the ZF background showed an improved leaf N partitioning with higher photosynthetic capacity parameter values (i.e. J_{max}, V_{cmax}, and T_p) (Table 3) and increased protein expression levels of Cyt b_6/f and Rubisco (Fig. 5), compared with its CK. A significant correlation as shown in Fig. 6 confirmed that higher Rubisco activity in the ZF-Y genotype came from more N investment in Rubisco-related proteins. Although leaf SLN of ZF-Y was increased obviously after stem-elongating stage, the significant increase in PNUE still confirmed the existence of this improvement (Table 4).

However, the process of improving N allocation was not observed in WYJ-Y. Given that both Y genotypes reduced N input to light-harvesting complexes (Fig. 5), where did the conserved N in WYJ-Y go? Medlyn (1996) suggested that leaf photosynthetic N content can be divided into four rate-limiting pools (i.e. chlorophyll, the electron transport system, Rubisco, and other soluble proteins). The four pools compete with each other for N in response to environmental changes (Yin et al., 2019). So the N resources saved from [CHL] in WYJ-Y are likely distributed over other soluble proteins that are not determining A_{max}, as no significant differences in components of the electron transport system and Rubisco were observed by our model- and proteomic-analysis (Table 3; Fig. 5). But photosynthetic N content generally differs among leaves and accounts for 50%–80% of total leaf N content in C_3 plants (Hikosaka and Terashima, 1995; Makino and Osmond, 1991). The leaf N allocated to photosynthesis-independent organelles or cell walls (Evans and Clarke, 2019) may have been the investment route for conserved N in the leaves of WYJ-Y. Any increased investment in respiration-related processes cannot explain this as R_d was even lower in WYJ-Y than in WYJ-CK (Table 3). Possible outlets concerning the saved N in WYJ-Y and whether the difference in photosynthetic behaviours between WYJ-Y and ZF-Y was due to genetic background would need more studies to elucidate.

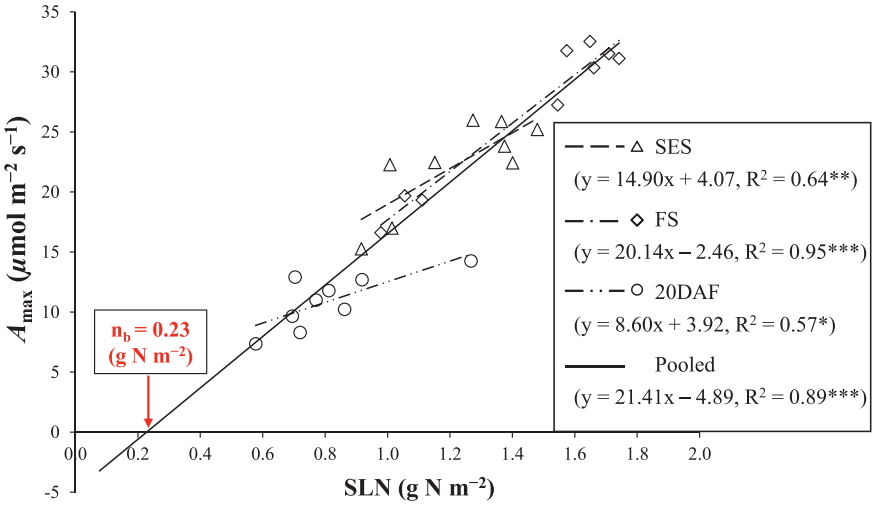

Fig. 7. Relationship between maximum photosynthesis rate (A_{max}) and specific leaf nitrogen (SLN). Data represented by different open shapes are from three stages (SES, stem-elongating stage; FS, flowering stage; and 20DAF, 20 d after flowering) in greenhouse experiment. Each point represents the mean of three or four replicates. Linear regressions were fitted for data for each stage and for pooled data, with the significance shown by asterisks (*P < 0.05, **P < 0.01, and ***P < 0.001). The extrapolation of the regression for the pooled data gave an estimate of the base leaf N for photosynthesis (n_b).

5. Conclusions

Altering leaf chlorophyll content can affect the photosynthetic physiology of the whole leaf. Overall, the G variants had little impact on photosynthesis until a very late stage towards maturity while larger effects were observed on Y variants due to significantly reduced [CHL], increased SLA and g_s, and high-light tolerance in Y variants, compared with their CK. Moreover, reducing [CHL] can prevent excessive absorption of solar radiation energy, resulting in little need to operate NPQ (i.e. low F_{npq}), but the key to change the inherent energy use mode is to translate the reduced NPQ into the energy demand of photochemical quenching by an increased photosynthetic capacity. Of the two Y variants analysed in this study, only ZF-Y showed a leaf N partitioning with improved photosynthetic capacity parameters (i.e. J_{max}, V_{cmax}, and T_p) and increased protein expression levels of Cyt b_6/f and Rubisco. Thus, both A_{max} and PNUE of ZF-Y were improved under saturated I_{inc}. The difference between WYJ-Y and ZF-Y might reflect the effect of genetic background, and the impact as observed in ZF is desirable as the Y variant from ZF background had advantages in photosynthesis under high-light environments. The results of our ZF materials confirmed the feasibility of reducing [CHL] of leaves coupled with distributing saved N into more beneficial investments on proteins that determine V_{cmax} and J_{max}. This provides a direction for breeding programmes or genetic engineering to improve leaf photosynthesis.

Abbreviations

Not applicable.

Availability of data and materials

Data will be shared upon request by the readers.

Authors' contributions

X.Y. and P.C.S. conceived the project; Z.Z. and X.Y. designed the research plan; Z.Z. performed the experiments with the help of PELvdP, J.G., and Z.W., analysed the data, and wrote the draft; X.Y., P.C.S., and J.Y. revised the manuscript. All authors commented on the manuscript and approved the final version.

Declarations of competing interest

The authors declare that they have no known competing financial interests or personal relationships that could have appeared to influence the work reported in this paper. Jianchang Yang and Xinyou Yin (Editorial Board members) were not involved in the journal's review nor decisions related to this manuscript.

Acknowledgements

Z.Z. thanks the China Scholar Council (CSC) for funding his PhD fellowship. We thank Dr. Changquan Zhang (Yangzhou University) and Prof. Fangmin Cheng (Zhejiang University) for providing seeds used in this study.

Appendix A. Supplementary data

Supplementary data to this article can be found online at https://doi.org/10.1016/j.crope.2023.02.001.

References

Arnon, D., 1949. Copper enzymes in isolated chloroplasts. Polyphenol oxidase in *Beta vulgaris*. Plant Physiol. 24, 1.
Bilger, W., Björkman, O., 1990. Role of the xanthophyll cycle in photoprotection elucidated by measurements of light-induced absorbance changes, fluorescence and photosynthesis in leaves of Hedera canariensis. Photosynth. Res. 25, 173–185.
Borrell, A.K., van Oosterom, E.J., Mullet, J.E., George-Jaeggli, B., Jordan, D.R., Klein, P.E., Hammer, G.L., 2014. Stay-green alleles individually enhance grain yield in sorghum under drought by modifying canopy development and water uptake patterns. New Phytol. 203, 817–830.
Chen, J., Liang, Y., Hu, X., Wang, X., Tan, F., Zhang, H., Ren, Z., Luo, P., 2010. Physiological characterization of "stay green" wheat cultivars during the grain filling stage under field growing conditions. Acta Physiol. Plant. 32, 875–882.
Cousins, A.B., Ghannoum, O., Von Caemmerer, S., Badger, M.R., 2010. Simultaneous determination of Rubisco carboxylase and oxygenase kinetic parameters in Triticum aestivum and Zea mays using membrane inlet mass spectrometry. Plant Cell Environ. 33, 444–452.
Cox, J., Mann, M., 2008. MaxQuant enables high peptide identification rates, individualized ppb-range mass accuracies and proteome-wide protein quantification. Nat. Biotechnol. 26, 1367–1372.
Cui, C., Wang, Z., Su, Y., Wang, T., 2021. New insight into the rapid growth of the Mikania micrantha stem based on DIA proteomic and RNA-Seq analysis. J. Proteomics 236, 104126.
Evans, J.R., 1996. Developmental constraints on photosynthesis: effects of light and nutrition. In: Baker, N. (Ed.), Photosynthesis and Environment. Springer, Dordrecht, pp. 281–304.
Evans, J.R., Clarke, V.C., 2019. The nitrogen cost of photosynthesis. J. Exp. Bot. 70, 7–15.
Evans, J.R., Poorter, H., 2001. Photosynthetic acclimation of plants to growth irradiance: the relative importance of specific leaf area and nitrogen partitioning in maximizing carbon gain. Plant Cell Environ. 24, 755–767.
Farquhar, G.D., von Caemmerer, S.V., Berry, J.A., 1980. A biochemical model of photosynthetic CO_2 assimilation in leaves of C_3 species. Planta 149, 78–90.
Genty, B., Briantais, J.M., Baker, N.R., 1989. The relationship between the quantum yield of photosynthetic electron transport and quenching of chlorophyll fluorescence. Biochim. Biophys. Acta-Gen. Subj. 990, 87–92.
Gilmore, A.M., Ball, M.C., 2000. Protection and storage of chlorophyll in overwintering evergreens. Proc. Natl. Acad. Sci. U.S.A. 97, 11098–11101.
Gilmore, A.M., Hazlett, T.L., Debrunner, P.G., Govindjee, 1996. Comparative time-resolved photosystem II chlorophyll a fluorescence analyses reveal distinctive differences between photoinhibitory reaction centre damage and xanthophyll cycle-dependent energy dissipation. Photochem. Photobiol. 64, 552–563.
Glick, R.E., Melis, A., 1988. Minimum photosynthetic unit size in system I and system II of barley chloroplasts. Biochim. Biophys. Acta-Bioenerg. 934, 151–155.
Gregersen, P.L., Culetic, A., Boschian, L., Krupinska, K., 2013. Plant senescence and crop productivity. Plant Mol. Biol. 82, 603–622.
Gu, J., Zhou, Z., Li, Z., Chen, Y., Wang, Z., Zhang, H., 2017a. Rice (*Oryza sativa* L.) with reduced chlorophyll content exhibit higher photosynthetic rate and efficiency, improved canopy light distribution, and greater yields than normally pigmented plants. Field Crops Res. 200, 58–70.
Gu, J., Zhou, Z., Li, Z., Chen, Y., Wang, Z., Zhang, H., Yang, J., 2017b. Photosynthetic properties and potentials for improvement of photosynthesis in pale green leaf rice under high light conditions. Front. Plant Sci. 8, 1082.
Harley, P.C., Loreto, F., Di Marco, G., Sharkey, T.D., 1992. Theoretical considerations when estimating the mesophyll conductance to CO_2 flux by analysis of the response of photosynthesis to CO_2. Plant Physiol. 98, 1429–1436.
Hendrickson, L., Furbank, R.T., Chow, W.S., 2004. A simple alternative approach to assessing the fate of absorbed light energy using chlorophyll fluorescence. Photosynth. Res. 82, 73–81.
Hikosaka, K., Terashima, I., 1995. A model of the acclimation of photosynthesis in the leaves of C_3 plants to sun and shade with respect to nitrogen use. Plant Cell Environ. 18, 605–618.
Hossain, M., Fischer, K.S., 1995. Rice research for food security and sustainable agricultural development in Asia: achievements and future challenges. Geojournal 35, 286–298.
Khush, G.S., 1995. Breaking the yield frontier of rice. Geojournal 35, 329–332.
Kirst, H., Gabilly, S.T., Niyogi, K.K., Lemaux, P.G., Melis, A., 2017. Photosynthetic antenna engineering to improve crop yields. Planta 245, 1009–1020.
Kirst, H., Shen, Y., Vamvaka, E., Betterle, N., Xu, D., Warek, U., Strickland, J., Melis, A., 2018. Downregulation of the $CpSRP_{43}$ gene expression confers a truncated light-harvesting antenna (TLA) and enhances biomass and leaf-to-stem ratio in *Nicotiana tabacum* canopies. Planta 248, 139–154.
Krieger-Liszkay, A., Fufezan, C., Trebst, A., 2008. Singlet oxygen production in photosystem II and related protection mechanism. Photosynth. Res. 98, 551–564.
Li, Y., Ren, B., Gao, L., Ding, L., Jiang, D., Xu, X., Shen, Q., Guo, S., 2013. Less chlorophyll does not necessarily restrain light capture ability and photosynthesis in a chlorophyll-deficient rice mutant. J. Agron. Crop Sci. 199, 49–56.
Liu, D., Wang, W., Cai, X., 2014. Modulation of amylose content by structure-based modification of Os GBSS 1 activity in rice (*Oryza sativa* L.). Plant Biotechnol. J. 12, 1297–1307.
Loriaux, S.D., Avenson, T.J., Welles, J.M., McDermitt, D.K., Eckles, R.D., Riensche, B., Genty, B., 2013. Closing in on maximum yield of chlorophyll fluorescence using a single multiphase flash of sub-saturating intensity. Plant Cell Environ. 36, 1755–1770.
Makino, A., Osmond, B., 1991. Effects of nitrogen nutrition on nitrogen partitioning between chloroplasts and mitochondria in pea and wheat. Plant Physiol. 96, 355–362.
Meacham, K., Sirault, X., Quick, W.P., von Caemmerer, S., Furbank, R., 2017. Diurnal solar energy conversion and photoprotection in rice canopies. Plant Physiol. 173, 495–508.
Medlyn, B.E., 1996. The optimal allocation of nitrogen within the C_3 photosynthetic system at elevated CO_2. Funct. Plant Biol. 23, 593–603.
Melis, A., 2009. Solar energy conversion efficiencies in photosynthesis: minimizing the chlorophyll antennae to maximize efficiency. Plant Sci. 177, 272–280.

Ort, D.R., Zhu, X., Melis, A., 2011. Optimizing antenna size to maximize photosynthetic efficiency. Plant Physiol. 155, 79–85.
Polle, J.E., Kanakagiri, S., Jin, E., Masuda, T., Melis, A., 2002. Truncated chlorophyll antenna size of the photosystems–a practical method to improve microalgal productivity and hydrogen production in mass culture. Int. J. Hydrogen Energy 27, 1257–1264.
Rotasperti, L., Tadini, L., Chiara, M., Crosatti, C., Guerra, D., Tagliani, A., Forlani, S., Ezquer, I., Horner, D., Hahns, P., Gajek, K., Pesaresi, P., 2022. The barley mutant happy under the sun 1 (hus1): an additional contribution to pale green crops. Environ. Exp. Bot. 196, 104795.
Ruban, A.V., 2016. Nonphotochemical chlorophyll fluorescence quenching: mechanism and effectiveness in protecting plants from photodamage. Plant Physiol. 170, 1903–1916.
Slattery, R.A., VanLoocke, A., Bernacchi, C.J., Zhu, X., Ort, D.R., 2017. Photosynthesis, light use efficiency, and yield of reduced-chlorophyll soybean mutants in field conditions. Front. Plant Sci. 8, 549.
Song, Q., Wang, Y., Qu, M., Ort, D.R., Zhu, X.G., 2017. The impact of modifying photosystem antenna size on canopy photosynthetic efficiency–development of a new canopy photosynthesis model scaling from metabolism to canopy level processes. Plant Cell Environ. 40, 2946–2957.
Song, Q., Zhang, G., Zhu, X.G., 2013. Optimal crop canopy architecture to maximise canopy photosynthetic CO_2 uptake under elevated CO_2–a theoretical study using a mechanistic model of canopy photosynthesis. Funct. Plant Biol. 40, 108–124.
Swain, D.K., Sandip, S.J., 2010. Development of SPAD values of medium-and long-duration rice variety for site-specific nitrogen management. J. Agron. 9, 38–44.
Takagi, D., Takumi, S., Hashiguchi, M., Sejima, T., Miyake, C., 2016. Superoxide and singlet oxygen produced within the thylakoid membranes both cause photosystem I photoinhibition. Plant Physiol. 171, 1626–1634.
Thomas, H., Ougham, H., 2014. The stay-green trait. J. Exp. Bot. 65, 3889–3900.
von Caemmerer, S., 2000. Biochemical Models of Leaf Photosynthesis. CSIRO Publishing, Australia.
Walker, B.J., Drewry, D.T., Slattery, R.A., VanLoocke, A., Cho, Y.B., Ort, D.R., 2018. Chlorophyll can be reduced in crop canopies with little penalty to photosynthesis. Plant Physiol. 176, 1215–1232.
Wood, C.W., Reeves, D.W., Himelrick, D.G., 1993. Relationships between chlorophyll meter readings and leaf chlorophyll concentration, N status, and crop yield: a review. Proc. Agron. Soc. N. Z. 23, 1–9.
Yin, X., Belay, D.W., van der Putten, P.E., Struik, P.C., 2014. Accounting for the decrease of photosystem photochemical efficiency with increasing irradiance to estimate quantum yield of leaf photosynthesis. Photosynth. Res. 122, 323–335.
Yin, X., Schapendonk, A.H., Struik, P.C., 2019. Exploring the optimum nitrogen partitioning to predict the acclimation of C_3 leaf photosynthesis to varying growth conditions. J. Exp. Bot. 70, 2435–2447.
Yin, X., Struik, P.C., Romero, P., Harbinson, J., Evers, J.B., Van Der Putten, P.E., Vos, J.A.N., 2009. Using combined measurements of gas exchange and chlorophyll fluorescence to estimate parameters of a biochemical C_3 photosynthesis model: a critical appraisal and a new integrated approach applied to leaves in a wheat (*Triticum aestivum*) canopy. Plant Cell Environ. 32, 448–464.
Yin, X., Sun, Z., Struik, P.C., Gu, J., 2011. Evaluating a new method to estimate the rate of leaf respiration in the light by analysis of combined gas exchange and chlorophyll fluorescence measurements. J. Exp. Bot. 62, 3489–3499.
Yin, X., van der Putten, P.E., Belay, D., Struik, P.C., 2020. Using photorespiratory oxygen response to analyse leaf mesophyll resistance. Photosynth. Res. 144, 85–99.
Zheng, H.J., Wu, A.Z., Zheng, C.C., Wang, Y.F., Cai, R., Shen, X.F., Xu, R.R., Liu, P., Kong, L.J., Dong, S.T., 2009. QTL mapping of maize (*Zea mays*) stay-green traits and their relationship to yield. Plant Breed. 128, 54–62.
Zhou, Y., Tan, Z., Xue, P., Wang, Y., Li, X., Guan, F., 2021. High-throughput, in-depth and estimated absolute quantification of plasma proteome using data-independent acquisition/mass spectrometry ("HIAP-DIA"). Proteomics 21, 2000264.